JOURNAL OF MATERIALS SCIENCE **39** (2004) 3329– 3337

Texture analysis of ancient coins with TOF neutron diffraction

YANXIA XIE
Department of Geology and Geophysics, University of California, 94720 Berkeley, California, USA

L. LUTTEROTTI
Department of Geology and Geophysics, University of California, 94720 Berkeley, California, USA; Dipartimento di Ingegneria dei Materiali, Università di Trento, 38050 Trento, Italy

H. R. WENK*, F. KOVACS
Department of Geology and Geophysics, University of California, 94720 Berkeley, California, USA
E-mail: wenk@seismo.berkeley.edu

Two ancient Greek coins were studied by time-of-flight (TOF) neutron diffraction to investigate their authenticity. Diffraction spectra were analyzed with the Rietveld programs GSAS and MAUD for phase proportions and texture. Both samples revealed very similar textures, consistent with pressing between dies. Also, both samples had similar phase proportions around 85% of silver and 15% of copper. The coin analysis revealed limitations of currently used processing methods for TOF neutron diffraction data. Despite the advantages of neutron diffraction for non-destructive bulk analyses, great care must be paid to the procedures to avoid artifacts. The conventional irregular and sparse coverage used at HIPD-LANSCE is problematic if absorption effects exist and the harmonic texture expansion is extended beyond $l_{max} = 6$. Direct texture methods, such as EWIMV, are less affected by coverage limitations and a new method to deal with absorption is introduced.

1. Introduction

Archaeologists, anthropologists and art historians often face the task to determine if an object is authentic or forged. Forgery is not just a recent problem [1] and scientific characterizations of archaeological materials have been pursued for some time [2]. Analytical techniques have become well established for this application, including gamma-radiography, laser-assisted Raman spectroscopy, neutron activation analysis, X-ray fluorescence, X-ray diffraction, and scanning electron microscopy. Large synchrotron and neutron facilities, which have mainly been devoted to research in physical sciences, have been applied to archaeological and historic objects [3–7].

In the present study, a pair of ancient Greek silver coins was studied by TOF neutron diffraction with HIPD (High Intensity Powder Diffractometer) at LANSCE (Los Alamos Neutron Science Center). Neutron, rather than X-ray or electron diffraction, was chosen because of the low attenuation of neutrons by matter which has the advantage that measurements are non-destructive and do not involve complicated sample preparations. Also, neutron diffraction analyzes bulk materials, rather than surfaces.

The two coins supposedly from Mesembria in the Thrace Black Sea region and dating to 450–350 BC were chosen for the analysis. Both have a similar appearance, though one is more tarnished than the other. The coins are classified as hemiobols with a facing helmet on the obverse side (Fig. 1) and a radial wheel on the reverse side (see Plate X 268-271 of [8]). One (we call it 2A) is a modern forgery prepared in Varna, Bulgaria. The second one (2B) is authentic. Quantitative texture analysis was applied to distinguish the original coin from its counterfeit, assuming that texture patterns would be different. In ancient times, metals were deformed by hammering, while today metal sheets are made by rolling or stamping. Both produce different crystal orientation patterns [9, 10]. Initially the study was intended as an archeological application of TOF neutron diffraction, but in the course of the analysis, some interesting methodological issues emerged and the study started to focus on the importance of various factors on the quality of TOF texture analysis. It became clear that details of data collection as well as data processing procedures could have a profound impact on results.

*Author to whom all correspondence should be addressed.

Figure 1 The two coins, 2B (left, authentic) and 2A (right, forgery) that were investigated. The actual size of the coins is 1 centimeter in diameter.

2. Measurements

For convenience, the two coins under investigation were labeled as 2A and 2B (Fig. 1). Their dimensions are disk-shaped, about 10 mm in diameter and 1.5 mm thick in the center. The neutron diffraction measurements were performed twice. The first measurements (in November 2000) simply had the archeological motivation in mind. The follow-up measurement (in July 2001) was carried out to reveal the degree of reproducibility and the influence of different measuring strategies on the results.

At LANSCE neutrons are produced by spallation. Protons with energies of 800 MeV are injected into a fast-cycling (300 ns) storage ring, compressing pulses to 250 ns. The intense proton bursts are then delivered to the Lujan Center at a frequency of 20 Hz and directed to a tungsten target to produce a short burst of high-energy neutrons by spallation. These high energy neutrons are then slowed down in a water moderator to thermal energies. The moderator is viewed by the HIPD diffractometer positioned on flight path 3 at the Lujan Center at a distance of 9 m from the moderator. With collimation a beam size of 2 cm $\times$ 1 cm is obtained at the sample with a flux of 10^7 n s^{-1} cm^{-2}.

HIPD has 8 detector banks ranging in diffraction angles from 14° to 153°. They are placed symmetrically on the two sides of the flight path in the horizontal plane to cover a large range of d-spacings ($\sim$0.25–$\sim$34 Å). The sample is mounted in a 2-circle goniometer that is placed in a vacuum chamber. The coins were mounted with their flat surfaces parallel to the goniometer χ circle (Fig. 2a). Thus in pole-figure space (Fig. 2b), the normal (N) to the coin's flat surface is in the vertical direction.

In the first measurements, both coins (2A and 2B) were measured with the same pole figure coverage, consisting of 13 pairs of randomly generated (ω, χ) angles [11]. The diffractions from the 13 sample orientations and 4 high angle (high resolution) detector banks ($\pm$153°, $\pm$90°), gives a total of 13 $\times$ 4 = 52 spectra with an irregular coverage (Fig. 3a). For some orientations and some detectors, the beam was totally or partly blocked by some instrument parts (mostly from the texture goniometer) and these spectra contain spurious peaks that are not from Bragg reflections of the coins. The regions in the spectra that contain these peaks (1.32–1.36, 1.62–1.66, 2.29–2.32 Å) were subsequently excluded from the analysis. Also, some detectors showed very weak count rates and were not used. To compensate for poor-quality spectra, spectra from the +40° bank were added to the analysis. Additional use of the +40° bank and the exclusion of the bad spectra resulted in a total of 53 spectra. The measurement time for coin 2A was 3 h (14 min at each orientation) and for coin 2B about 4 h (20 min at each orientation).

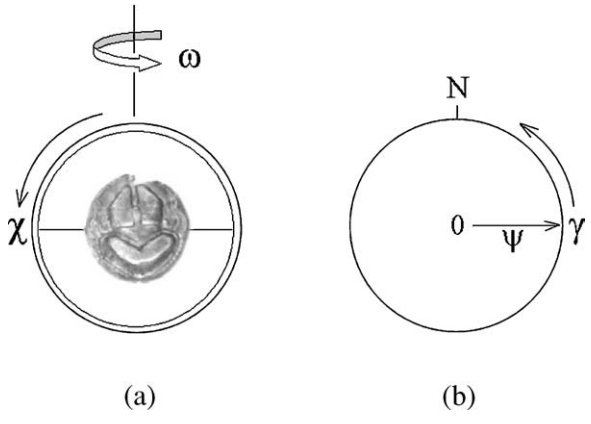

Figure 2 The experimental setting and its relation with the pole figure space. (a) The mounting geometry of the coins on the HIPD texture goniometer, with the beam being parallel to the χ circle normal. (b) Pole figure space with the normal (N) to the coin's flat surface in the vertical direction.

In the second measurement, only coin 2B was measured with a regular hexagonal equal area coverage [12]), consisting of 71 (ω, χ) rotational settings, using first only bank 3 (+90°) (Fig. 3b). The pole figure was covered with measurements from the center to a pole distance of 70° and half of the ring at the periphery (90°). The total measurement time in the second round was about 20 h (17 min at each orientation). Later, for some aspects of the analysis, data from the other high angle banks were added ($\pm$153°, $-$90°) but excluding spectra with spurious peaks. The total number of spectra used in this analysis was 122.

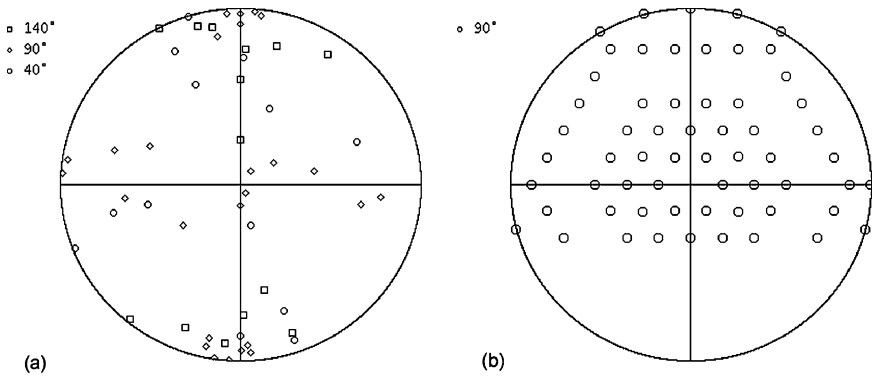

Figure 3 Pole figure coverages for the two sets of measurements. (a) Irregular coverage from the first measurements (using ±153°, ±90° banks, different banks indicated with symbols); (b) regular hexagonal coverage from the second measurements (using only +90° bank). Equal area projection.

3. Rietveld texture analysis

With constant wavelength neutron diffraction, i.e., at a reactor source, individual pole figures *hkl* are measured. The three-dimensional orientation distribution function (ODF) that describes the texture is obtained from complete or incomplete pole figures with various mathematical methods [13]. However, with TOF neutron diffraction complete spectra with many diffraction peaks, rather than individual peaks, are recorded. Therefore it is more efficient to extract texture information directly from the whole diffraction spectrum. By taking advantage of the well-developed Rietveld scheme [14, 15], which determines crystal structures based on the whole diffraction spectrum, texture researchers have started to incorporate quantitative texture analysis in the Rietveld method. The ODF computations are performed either in Fourier space (series expansion or harmonic methods) or directly in orientation space (direct or discrete methods). Direct methods have been applied to several geological materials such as calcite [16, 17], eclogite [18] and plagioclase [19], documenting advantages of TOF neutron diffraction in combination with the Rietveld method for low-symmetry and multi-phase materials with complicated diffraction spectra. At least two software packages are available that implement texture analysis in the Rietveld method: MAUD (Material Analysis Using Diffraction [20]) and GSAS (General Structure Analysis System [11, 21]). Regarding texture analysis, MAUD implements both direct methods and the spherical harmonic method. GSAS only uses the harmonic method.

In the coin project we relied mainly on the spherical harmonic method for two reasons: First, we wanted to directly compare two different approaches (GSAS and MAUD). Secondly we wanted to explore the influence of the degree of the harmonic expansion on the resolution of the texture. For one sample (2B) we also applied the discrete method in MAUD.

Fig. 4 displays 4 spectra from the first measurement collected at different sample orientations with the +90° detector. It is noticeable that relative peak intensities are slightly different for different sample orientations, indicating the existence of a weak texture.

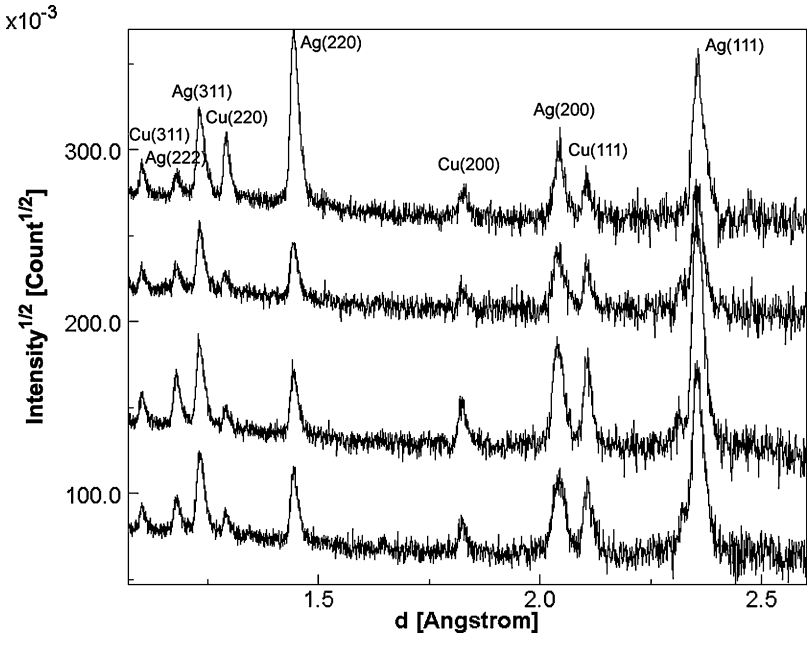

Figure 4 4 spectra from different sample orientations (first measurement data set) for coin 2B. The relative intensities of diffraction peaks at different sample orientations are different, showing the presence of preferred orientation. Some diffraction peaks are indexed.

The usable spectra were entered into GSAS and MAUD for analysis. The high-quality portion of the spectra, (d-range of 0.6–2.6 Å) was chosen for calculation. For the phase information, on the first try, the crystal-structure information of silver, guessed from the appearance of the coins, was taken as input. The phase silver matched successfully part of the peaks of the experimental spectra of both 2A and 2B. The remaining peaks could be explained with copper.

The analytical procedure is similar in GSAS and MAUD. First the instrument, crystal structural parameters, and phase volume fractions were refined. In GSAS, they are zero offset (5, one for each detector), histogram scale factors (53 parameters), background coefficients (53×4), lattice parameters (2), profile coefficients (18), absorption coefficients (53) and phase volume fractions (1). In MAUD, they are zero offset (5), histogram scale factors (53), background coefficients (5×5), lattice parameters (2), crystal size (2), microstrain (2), and phase volume fraction (1). With both programs scale factors for all individual spectra were refined to account for the absorption anisotropy due to the aspherical shape of the coins. In a second analysis attempt absorption was modeled in MAUD by introducing a suitable model and nine associated sample shape coefficients were refined, rather than individual scale factors. In this manner the number of refinable scale/absorption parameters has been decreased to 9 from 106 improving the convergence of the solution (see discussion below).

After these Rietveld parameters were established, the texture refinement was activated. For the spherical harmonic model, the refinable texture parameters are the harmonic coefficients (22 for harmonic degree 6 and 110 for harmonic degree 12 for each phase). No sample symmetry was assumed for the texture refinement. For the direct texture method the EWIMV algorithm was used in MAUD. This approach requires no additional least squares parameters as it relies on extracted texture factors and uses its own maximum entropy optimization algorithm. The EWIMV method is an extension of the WIMV method explicitly developed for the Rietveld analysis to take into consideration points that are irregularly distributed over orientation space which is a limitation of the conventional WIMV method [22] that requires a regular coverage normally achieved through interpolation of the extracted pole figure values.

MAUD outputs directly the pole figures and the ODF; (100), (110) and (111) pole figures were recalculated for plotting. For GSAS pole figures were calculated for the d-spacing range of 0.6–2.6 Å. The first 13 of these complete pole figures for both phases were then used as input for the conventional WIMV analysis in BEARTEX [23] to obtain the ODF and then (100), (110), and (111) pole figures were recalculated from the ODF. As a note of caution, in GSAS, if the positive pole figure constraint is used, all negative values are set to zero and compatibility between pole figures is not guaranteed.

4. Results

Both coins, 2A and 2B, were found to be composed of two fcc phases: silver and copper as the fit of observed spectra indicates (Fig. 5). The refined lattice parameters and the phase proportions are listed in Table I. Note that for TOF methods absolute values of lattice parameters are very sensitive to sample alignment and instrument calibration. In this study absolute values are not important since emphasis is on the comparison of relative values obtained with different methods for the same data. The results for lattice parameters from MAUD and GSAS are identical within experimental errors that are underestimated from the standard deviations. Also results for phase proportions of coin 2A and coin 2B are similar. However, MAUD yielded always a smaller copper content compared to GSAS and both programs suggest a slightly higher silver content for coin 2A. The discrepancy can be explained by noting that the phase contents reported for GSAS were obtained with the harmonic method, whereas those for MAUD rely on EWIMV and an absorption model.

Fig. 6 shows pole figures for silver and copper for coins 2A and 2B, analyzed with GSAS and harmonic expansion to $l_{\max} = 6$. The principal feature in all pole figures is a (110) fiber parallel to the coin normal (top in the pole figures). This is the typical texture component for axial compression of fcc metals [e.g., 9, 10]. Approximate axial symmetry is observed but with some significant deviations expressed in subsidiary maxima and minima on the small circle girdles (some indicated by arrows in Fig. 6). Interestingly these same deviations are present for both phases (silver: Fig. 6a, b, copper Fig. 6c, d) and for both samples (2A Fig. 6a, c and 2B Fig. 6b, d). This suggests that they may be an artifact of the texture analysis and we suspected that the highly irregular coverage (Fig. 3a) could be the cause. This was the motivation for conducting a second set of measurements with a different strategy (only for coin 2B). Indeed, analysis of data for incomplete but regular coverage, and only using the $+90^\circ$ detector bank (Fig. 3b), produces for the same conditions pole figures that are much closer to axially symmetric (Fig. 7).

It thus appeared that coverage was not sufficient to constrain the oscillations of the harmonic functions in the first set of measurements. To test this hypothesis we assumed a hypothetical fiber texture based on ideal components and generated with MAUD corresponding diffraction spectra for the coverage of the first measurements, using instrument parameters for the real spectra and imposing a small scatter function. With these synthetic spectra we recalculated the ODF by Rietveld analysis of the artificial data and from that the pole figures. We do not show results here, but the recalculated texture was identical with the initial model texture. This demonstrated on one hand that the numerical procedure was correct, and on the other hand that coverage alone is not responsible for the artifacts in Fig. 6.

In a next iteration we turned our attention to absorption. Indeed, silver is a high neutron absorber ($\mu = 2.1$ cm^{-1} for $\lambda = 1.08$ Å) compared to copper ($\mu = 0.19$ cm^{-1}). A simple estimation of absorption for the sample dimensions suggests that the average path length for incident and diffracted beam in the sample is 6 mm if the coin normal is parallel to the incident beam and perpendicular to the 90° detector, and 4 mm if it is at 45°. For

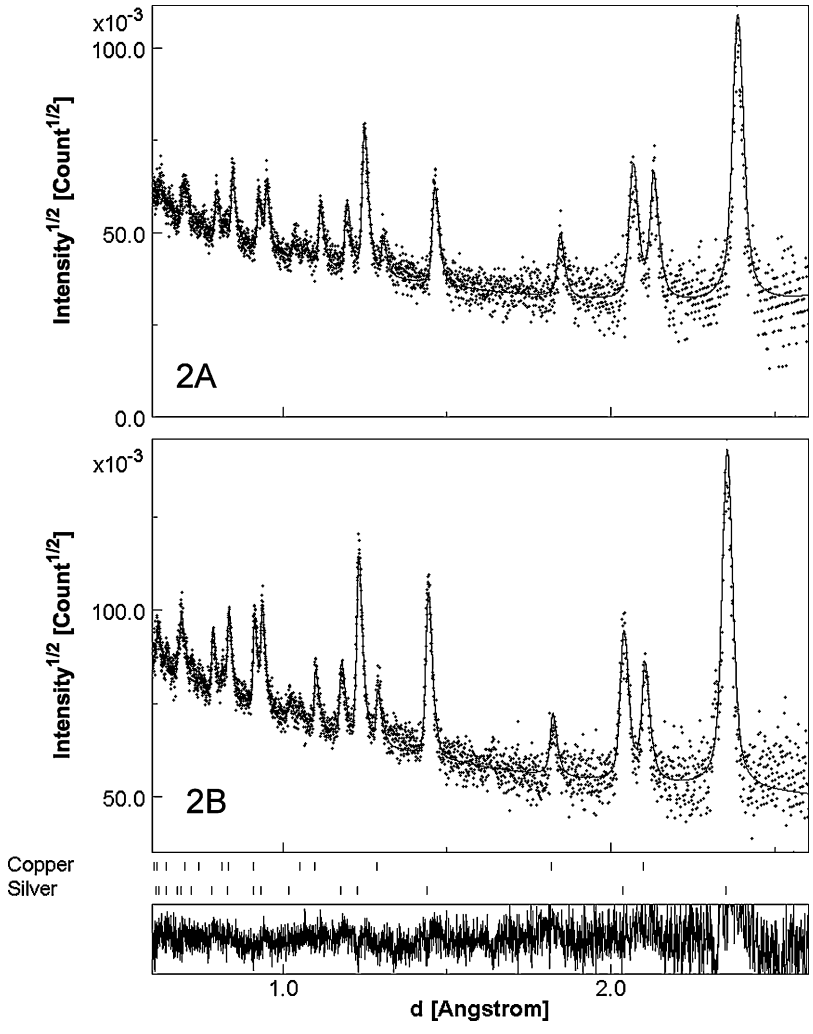

Figure 5 Rietveld fits of coin 2A (upper) and 2B (bottom), for the two phases silver and copper. Diffraction peaks of both phases are marked below the spectra. The displayed range corresponds to that used in the refinements.

a reflection 111 the corresponding absorption reduces the intensity for the two cases to approximately 15 and 31% respectively. Indeed, for the second measurement we noticed that refined scale factors varied by a similar amount and a plot of scale factors (Fig. 8a) reflects the general coin geometry, with small scale factors (high absorption) on small circles at 45° to the coin normal. It became clear that a combination of the irregular coverage, with detectors of different sensitivities, experimental errors, high absorption and the harmonic method was the reason for the artifacts observed in Fig. 6.

To further investigate these complications and to develop a more advanced absorption correction procedure we analyzed the data with the Rietveld code MAUD. If the same data for the first set of measurements are used and the same parameters refined as we did with GSAS (scale factors for all spectra), then we get for the harmonic method and $l_{\max} = 6$ similar results as for GSAS (Fig. 9a), with subsidiary maxima, particularly along 45° small circles. In fact deviations are larger if the refinement is performed to full convergence, which is slow. A representation with $l_{\max} = 6$ is only applicable to very weak textures and to test the possibility of using higher harmonic orders, as is commonly done in X-ray texture analysis, we calculated textures for $l_{\max} = 12$ (Fig. 9b). Already for $l_{\max} = 12$ unrealistic

TABLE I Refined lattice parameters and volume fraction of phases. Estimated standard deviations are in parentheses (in Maud only one volume fraction is refined, the other is computed as complement to the whole)

		Phase proportion (vol%)		*a* (Å)	
Coin	Phase	MAUD	GSAS	MAUD	GSAS
2A	Silver	87.9	82.6 (8)	4.0763 (1)	4.0787 (2)
	Copper	13.1 (1)	17.4 (8)	3.6366 (1)	3.6386 (2)
2B	Silver	90.4	86.5 (7)	4.0677 (1)	4.0722 (1)
First measurement	Copper	9.6 (1)	13.5 (7)	3.6364 (1)	3.6389 (2)
Second measurement	Silver	92.0	87.3 (2)	4.0872 (1)	4.0728 (1)
	Copper	8.0 (1)	12.7 (2)	3.6513 (1)	3.6402 (1)

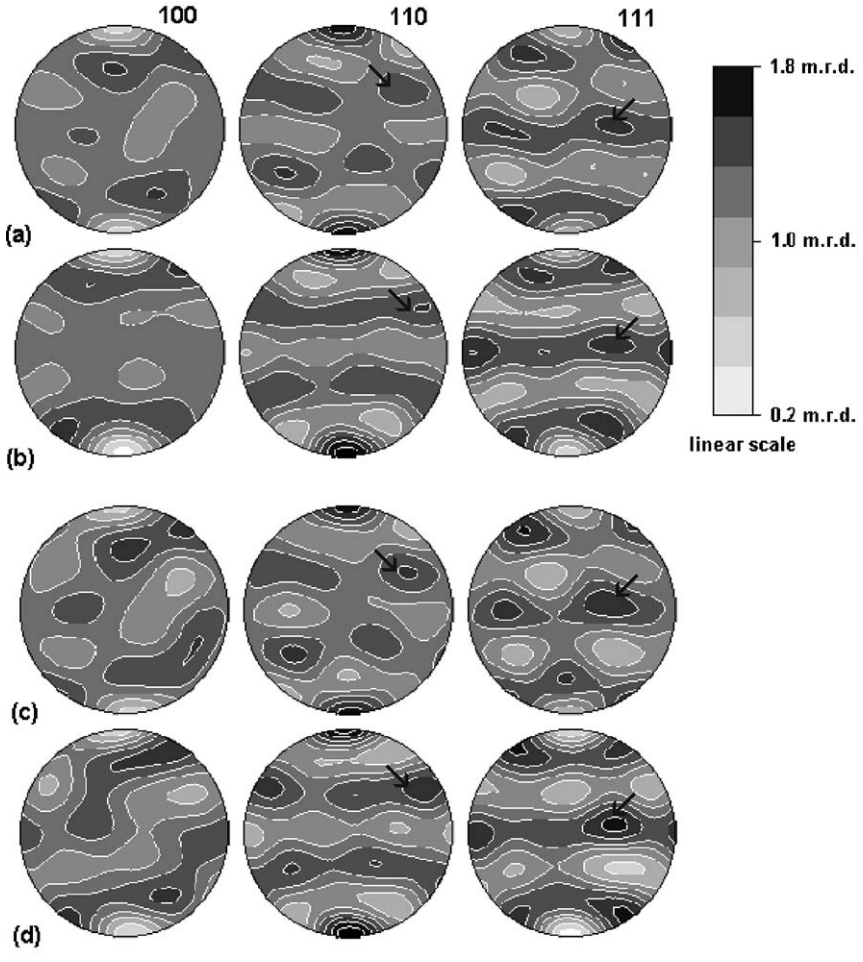

Figure 6 Principal pole figures, (100), (110), (111), of silver (a,b) and copper (c,d) in both coin 2A (a,c) and 2B (b,d), calculated by GSAS for the first set of measurements and $l_{max} = 6$. Equal area projection, linear contour intervals. Note that the same contour system is used for all following pole figures to allow for direct comparison.

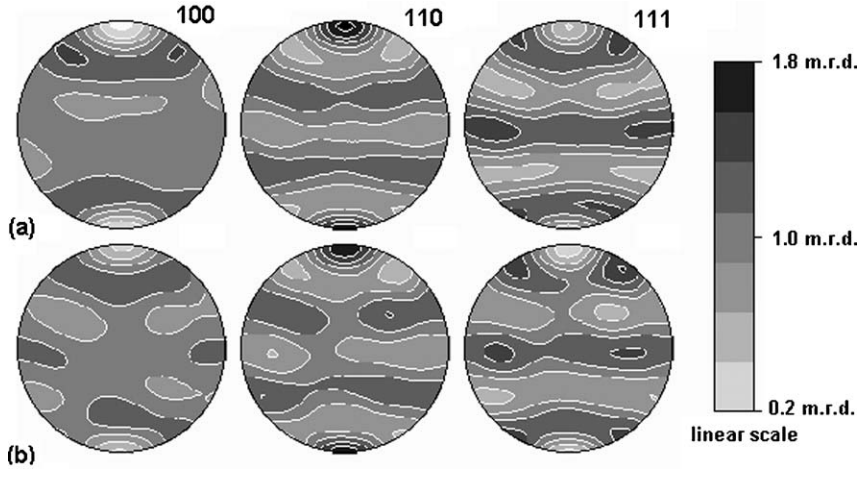

Figure 7 Principal pole figures, (100), (110), (111), of silver (a) and copper (b) of coin 2B, calculated by GSAS and $l_{max} = 6$ for the second (regular) measurement data. Equal area projection, linear contour intervals.

oscillations develop indicating that the standard pole figure coverage for HIPD is not sufficient for quantitative texture analysis using the harmonic method of even moderately strong textures.

Next the analysis for the first coverage (Fig. 3a) was performed using an absorption model and the EWIMV method instead of the harmonic one to compute the ODF for the first set of measurements. A large ODF cell size of 15° coupled with the use of the tube projection feature was used for the analysis to compensate for the large holes in the measurement coverage. Since the texture is sufficiently smooth a smaller cell size is not necessary. With this method subsidiary maxima are less pronounced and the texture represented in the recalculated pole figures of Fig. 10 is in fair agreement with the one obtained from the second measurement with a regular coverage and analysed by the spherical harmonic method (Fig. 7), though the calculated texture is

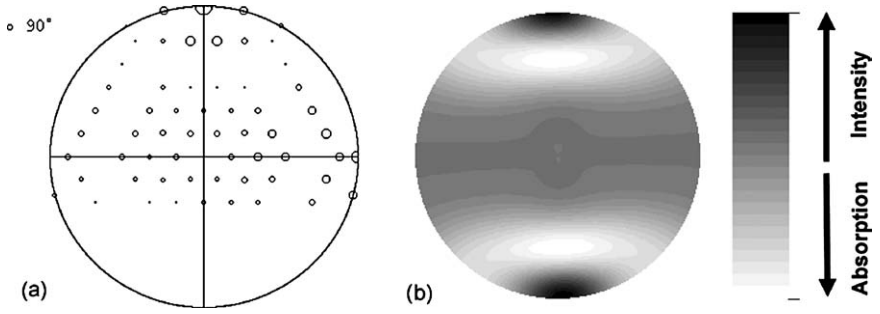

Figure 8 (a) Refined histogram scale factors for the second set of measurements. Large scale factors (low absorption) are indicated by large symbols. (b) Absorption factor surface based on 8 harmonic coefficients for the $+90^\circ$ detector and the first set of measurements. A low value indicates high absorption. Both diagrams are in pole figure space and the same orientation as pole figures with the coin normal on top.

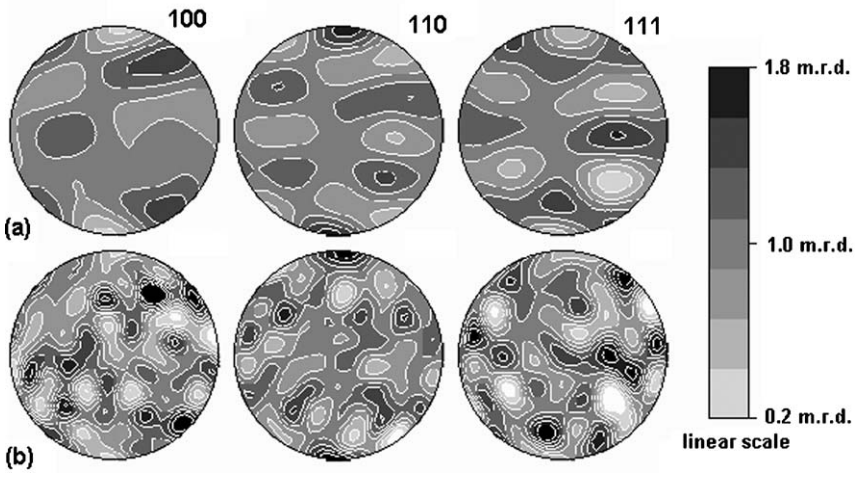

Figure 9 Principal pole figures, (100), (110), (111) for silver of coin 2B, calculated by MAUD with the harmonic method for the first set of measurements and $l_{\max} = 6$ (a) and $l_{\max} = 12$ (b). Equal area projection, linear contour intervals.

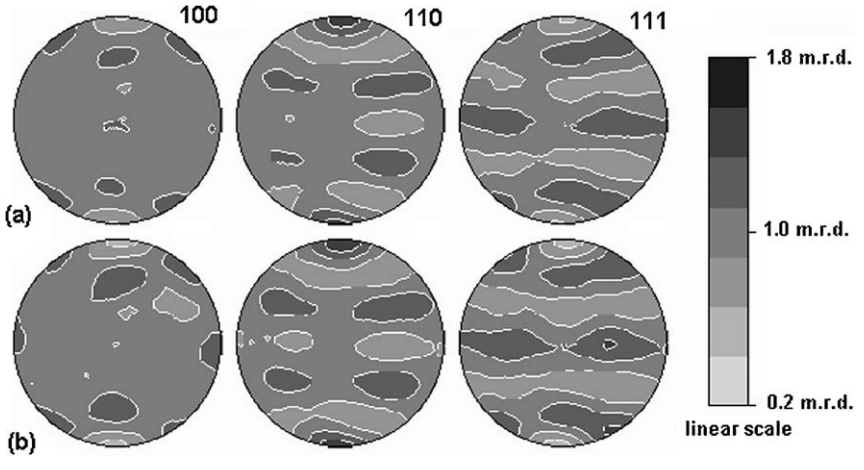

Figure 10 Principal pole figures, (100), (110), (111), of silver (a) and copper (b) of coin 2B, calculated by MAUD with the EWIMV method and refining an absorption model for the first measurement data. Equal area projection, linear contour intervals.

considerably weaker. For this analysis in Maud we introduced an approximate absorption model to account for the change in scale factors through rotation of the sample as described previously. The model developed makes use of a harmonic expansion treatment for the approximation of the general shape of a grain, based on the Laue crystal group of the sample shape [24]. We used here the same concept to describe the shape of the coin, approximating it with a certain number of coefficients. From the shape we can compute the absorption path of a neutron particle traveling and scattered inside the sample. From the path it is easy to compute the intensity absorbed by the sample for a certain orientation. The model has been incorporated in the Rietveld program MAUD and the harmonic coefficients describing the shape have been refined by least squares. It should be noted that the shape obtained may not correspond exactly to the true shape of the coin, as we are just refining absorption characteristics. With this method we are using fewer parameters than refining one scale factor and an absorption parameter for each spectrum, thus improving the convergence of the analysis. The shape

anisotropy absorption model was successful to refine the spectra to a comparable accuracy as in the previous analyses despite the use of a much smaller number of variable parameters. In some cases the fit was even better, probably due to the reduced number of variables that permitted a better convergence of the solution. The absorption correction computed by the model for the detector at $+90^\circ$ is shown in Fig. 8b and is comparable with scale factors refined in the second measurement (Fig. 8a).

5. Discussion

The results show that both coins were composed of between 85 and 90 vol% of silver and the rest in copper. Both phases in both samples developed a weak (110) fiber texture, which is the typical texture for fcc materials deformed in axial compression [9, 10]. It indicates that neither with phase proportions nor texture patterns can we distinguish between the two coins. The observed texture is consistent with ancient practice to produce coins by striking between two dies.

Therefore, no conclusions can be drawn about the authenticity of the coins. The fact that they are composed of a mixture of silver and copper is typical of ancient metallurgy [25]. Interestingly an energy-dispersive X-ray analysis in the scanning microscope revealed that the surface is almost pure silver and that copper is present instead in the interior. It has been common practice to enrich the surface in precious metals by bathing objects in a brine to deplete base metals. Obviously the ancient as well as the modern coin were struck with a similar technique to produce the same texture. It should be mentioned that neutron exposure may alter the isotopic composition of artifacts significantly to make them unsuitable for later investigations.

The analysis of these coins revealed new information about details of quantitative texture analysis with neutrons and the Rietveld method that are of general interest. It was reassuring to see that the two software packages GSAS and MAUD, gave similar results for the same boundary conditions. Each of the software packages has its advantages and disadvantages. GSAS, written largely in FORTRAN and using an analytical formulation of derivatives, is computationally fast. However, the analytical formulation makes it difficult to deal with empirical non-linear functions that are used to describe instrument capabilities and microstructural characteristics. For texture analysis GSAS only uses the harmonic method, without consideration of ghost correction [26, 27]. GSAS only runs on SG-Irix, Linux, HPUX, and MS-DOS. In MAUD derivatives are calculated numerically and this makes the procedure much slower but also gives much greater flexibility. Several methods of texture analysis are implemented in MAUD, including harmonic [28], WIMV [22], and maximum entropy [29]. The entire program is written in JAVA and runs on any platform supporting this standard, such as MS-Windows, Unix, Linux, Mac OS and Mac OS X, and MAUD can be run over the network (Java Webstart). In addition, MAUD has an automatic mode for a complete analysis without user interaction as well as a manual mode with many additional options.

The texture simulation analysis shows that the pole figure coverage alone is not the cause of artifacts in the texture solutions. But for real data with experimental errors, counting statistics, absorption, different detector efficiencies and resolution, the harmonic method (even when the truncation of the series expansion is of low order $l_{\max} = 6$ or 8) is limited within the Rietveld concept. While the spherical harmonic method can handle irregular coverage, meaningful values of pole figure coefficients cannot be obtained for larger $l_{\max}$. For $l_{\max} = 6$ resolution is poor ($\approx 360^\circ/(\sqrt{2}\, l_{\max})$, [30]) and only sufficient to represent very weak textures. While the original idea behind the Rietveld concept was to use few orientations and many diffraction peaks, it has become apparent that a minimum coverage is still required, particularly in the case of cubic crystal symmetry, where the number of independent diffraction peaks is limited. It turns out that discrete methods (such as EWIMV) are less limited by irregular coverage.

If samples are highly unequiaxed and have significant absorption, a sophisticated absorption correction is required, particularly in view of the energy dependence of the absorption coefficient for polychromatic neutrons. Simply refining a scale factor for each spectrum is generally inadequate, because this scale factor also depends on detector efficiency, variations in incident beam intensity and texture. A combination of these uncertainties is the reason for the artifacts that we observed. This is compounded by the fact that the phase distribution in the coins is heterogeneous, which has not been taken into account in the absorption correction procedure described here.

6. Conclusions

TOF neutron diffraction is advantageous to characterize the features of archaeological materials due to its non-destructive nature. The textures of a pair of ancient coins have been determined by quantitative Rietveld texture analysis and similar textures were found in both samples, each composed of two fcc phases, silver and copper. The analysis packages GSAS and MAUD gave similar results for the harmonic method but revealed limitations of resolution for irregular coverage if a higher series-truncation value is used. Direct methods, as implemented in MAUD, are less susceptible to coverage limitations if proper absorption corrections are applied.

Acknowledgements

We are appreciative for help from R. Von Dreele and P. Encinias. Reviews by S. Vogel and an anonymous referee improved the manuscript. The research was supported by NSF, IGPP-LANL and UCDRD-LANL.

References

1. M. S. LESNEY, *Today's Chem. Work* **11** (2002) 22.
2. M. MANTLER and M. SCHREINER, *X-ray Spectrometry* **29** (2000) 3.
3. W. KOCKELMANN, A. KIRFEL and E. HÄHNEL, *J. Archaeol. Sci.* **28** (2001) 213.

4. K. JANSSENS, G. VITTIGLIO, I. DERAEDT, A. AERTS, B. VEKEMANS, L. VINCZE, F. WEI, I. DERYCK, O. SCHALM, F. ADAMS, A. RINDBY, A. KNÖCHEL, A. SIMIONOVICI and A. SNIGIREV, *X-ray Spectrometry* **29** (2000) 73.
5. P. WALTER, P. MARTINETTO, G. TSOUCARIS, R. BRENIAUX, M. A. LEFEBVRE, G. RICHARD, J. TALABOT and E. DOORYHÉE, *Nature* **397** (1999) 483.
6. A. P. J. STAMPFL, E. S. FRIEDMAN, T. J. WILKINSON, E. E. ALP and K. A. YENER, *Nucl. Instrum. Meth. Phys. Res.* A **467/468** (2001) 1305.
7. C. C. TANG, E. J. MACLEAN, M. A. ROBERTS, D. T. CLARKE, E. PANTOS and A. J. N. W. PRAG, *J. Archaeol. Sci.* **28** (2001) 1015.
8. "Sylloge Nummorum Graecorum," Vol. 9 (British Museum Press, 1993) Part 1.
9. H. HU, *Texture* **1** (1974) 233.
10. A. D. ROLLETT and S. I. WRIGHT, in "Texture and Anisotropy, Preferred Orientations in Polycrystals and Their Effect on Materials Properties," edited by U. F. Kocks, C. N. Tomé and H.-R. Wenk (Cambridge University Press, Cambridge, 1998) p. 178.
11. R. B. VON DREELE, *J. Appl. Cryst.* **30** (1997) 517.
12. S. MATTHIES and H.-R. WENK, *Phys. Stat. Sol.* A **133** (1992) 253.
13. J. S. KALLEND, in "Texture and Anisotropy, Preferred Orientations in Polycrystals and their Effect on Materials Properties," edited by U. F. Kocks, C. N. Tomé and H.-R. Wenk (Cambridge University Press, Cambridge, 1998) p. 102.
14. H. M. RIETVELD, *J. Appl. Cryst*. **2** (1969) 65.
15. R. A. YOUNG, "The Rietveld Method" (Oxford University Press, Oxford, 1993).
16. L. LUTTEROTTI, S. MATTHIES, H.-R. WENK, A. J. SCHULTZ and J. W. RICHARDSON, *J. Appl. Phys.* **81** (1997) 594.
17. H.-R. WENK, L. CONT, Y. XIE, L. LUTTEROTTI, L. RATSCHBACHER and J. RICHARDSON, *J. Appl. Cryst*. **34** (2001) 442.
18. Y. XIE, H.-R. WENK and S. MATTHIES, *Tectonophysics* **370** (2003) 269.
19. H.-R. WENK, LUTTEROTTI and S. VOGEL, *S. Nucl. Instr. Methods* A **515** (2003) 575.
20. L. LUTTEROTTI, S. MATTHIES and H.-R. WENK, in Proceeding of the Twelfth International Conference on Textures of Materials ICOTOM-12, Montreal 1999, edited by J. A. Szpunar (NRC Research Press, Ottawa, 1999) p. 1599.
21. A. C. LARSON and R. B. VON DREELE, "GSAS, General Structure Analysis System" (Los Alamos National Laboratory Report LAUR86-748, 1986).
22. S. MATTHIES and G. VINEL, *Phys. Stat. Sol.* B **112** (1982) K111.
23. H.-R. WENK, S. MATTHIES, J. DONOVAN and D. CHATEIGNER, *J. Appl. Cryst*. **31** (1998) 262.
24. N. C. POPA, *ibid.* **31** (1998) 176.
25. J. BAKER and M. PONTING, *The Numism. Chron.* **161** (2001) 207.
26. S. MATTHIES, *Phys. Stat. Sol.* B **92** (1979) K135.
27. M. DAHMS and H. J. BUNGE, *Text. Microstr.* **10** (1988) 21.
28. H.-J. BUNGE, *Z. Metallk*. **56** (1965) 872.
29. H. SCHAEBEN, *Phys. Stat. Sol.* B **148** (1988) 63.
30. H.-R. WENK, K. PAWLIK, J. POSPIECH and J. S. KALLEND, *Text. Microstr.* **22** (1994) 233.

Received 5 June 2003
and accepted 28 January 2004